JACS Au
AN OPEN ACCESS JOURNAL OF THE AMERICAN CHEMICAL SOCIETY

pubs.acs.org/jacsau

Article

Heterochiral Diastereomer-Discriminative Diphanes That Form Hierarchical Superstructures with Nonlinear Optical Properties

Jiaolong Chen, Zhenyu Yang, Gucheng Zhu, Enguang Fu, Pan Li, Fangyi Chen, Chunyang Yu, Shiyong Wang, and Shaodong Zhang*

Cite This: *JACS Au* 2022, 2, 1661−1668

Read Online

ACCESS | Metrics & More | Article Recommendations | Supporting Information

ABSTRACT: In order to study the emergence of homochirality during complex molecular systems, most works mainly concentrated on the resolution of a pair of enantiomers. However, the preference of homochiral over heterochiral isomers has been overlooked, with very limited examples focusing only on noncovalent interactions. We herein report on *diastereomeric discrimination* of twin-cavity cages (denoted as *diphanes*) against heterochiral tris-(2-aminopropyl)amine (TRPN) bearing triple stereocenters. This *diastereomeric selectivity* results from distinct spatial orientation of reactive secondary amines on TRPN. Homochiral TRPNs with all reactive moieties rotating in the same way facilitate the formation of homochiral and achiral *meso diphanes* with low strain energy, while heterochiral TRPNs with uneven orientation of secondary amines preclude the formation of cage-like entity, since the virtual *diphanes* exhibit considerably high strain. Moreover, homochiral *diphanes* self-assemble into an acentric superstructure composed of single-handed helices, which exhibits interesting nonlinear optical behavior. Such a property is a unique occurrence for organic cages, which thus showcases their potential to spawn novel materials with interesting properties and functions.

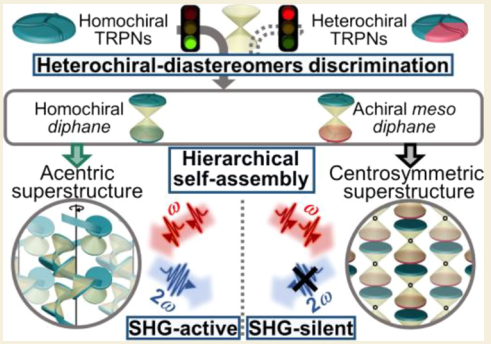

KEYWORDS: *cage-like compounds, diastereomeric selectivity, diphanes, hierarchical self-assembly, second-harmonic generation, superstructures*

INTRODUCTION

Life employs chirality as a pervasive tool from molecular to macroscopic scales to realize self-reproduction and physiological functions,[1] and yet the selection of homochirality remains mysterious.[2] Since Pasteur's seminal work on chiral resolution of enantiomers from tartrate racemates during crystallization,[3] numerous artificial systems have been developed for a mechanistic interpretation of emergence of homochirality in molecular[4] and supramolecular[5] levels. The majority of these works focused on deracemization and/or chiral resolution from a pair of enantiomers. On the other hand, how homochiral isomers are favored over their heterochiral counterparts in multiple diastereomer-containing systems has been rarely studied,[6] and the insofar limited examples exclusively exploited noncovalent interactions.

In the present work, we have devised a model study to investigate if nonchiral molecules can distinguish homochiral isomers from their heterochiral analogues. To this end, a nonchiral hourglass-like hexa-aldehyde precursor is chosen to react with tris-(2-aminopropyl)amine (TRPN) bearing three chiral centers, which might form a twin-cavity cage denoted as *diphane* (Figure 1).[7] An organic cage[8] is deemed as an ideal model for such a purpose: (i) the reversible nature of dynamic covalent chemistry (DCC) involved in its synthesis favors the formation of the thermodynamic product; (ii) its formation results from a delicate interplay between its three-dimensional framework and the spatial orientation of the multiple stereocenters within TRPN. By using experimental and theoretical approaches, we will elucidate the rationale behind the selective formation of homochiral *diphanes* and their achiral *meso* counterpart.

We also investigate the self-assembly of homochiral and achiral *diphanes*, which serve as supramolecular building blocks for the construction of hierarchical superstructures. With the aids of single-crystal X-ray diffraction (SC-XRD) and circular dichroism (CD), we reveal that this configurational change of the cages yields superstructures with dramatically different molecular packing.[9] It in turn results in distinct emergent functions, as demonstrated by their second-order nonlinear optical (NLO) properties as a proof of concept (Figure 1).

Received: April 12, 2022
Revised: May 25, 2022
Accepted: May 25, 2022
Published: July 12, 2022

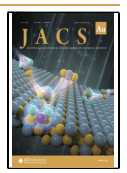

https://doi.org/10.1021/jacsau.2c00225
JACS Au 2022, 2, 1661−1668

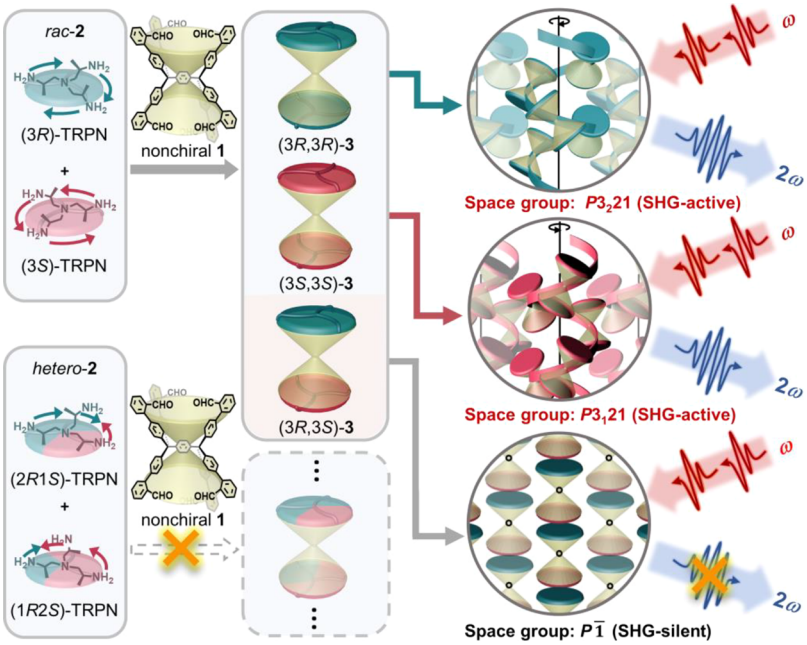

Figure 1. Selective formation of three *diphanes*, their self-assembly behavior in the crystalline phase, and different second-harmonic generation (SHG) responses. Nonchiral hexa-aldehyde compound **1** only reacts with racemic triamine *rac*-**2** ((3*R*)-TRPN: (3*S*)-TRPN = 1:1), rather than *hetero*-**2** ((2*R*1*S*)-TRPN : (1*R*2*S*)-TRPN = 1:1), to yield (3*R*,3*R*)-**3**, (3*S*,3*S*)-**3** and (3*R*,3*S*)-**3**. Chiral *diphanes* (3*R*,3*R*)-**3** and (3*S*,3*S*)-**3** crystallize into noncentrosymmetric trigonal space group $P3_221$ and $P3_121$ with active SHG response, whereas achiral *meso diphane* (3*R*,3*S*)-**3** crystallizes into centrosymmetric triclinic space group $P\bar{1}$ that is SHG-silent.

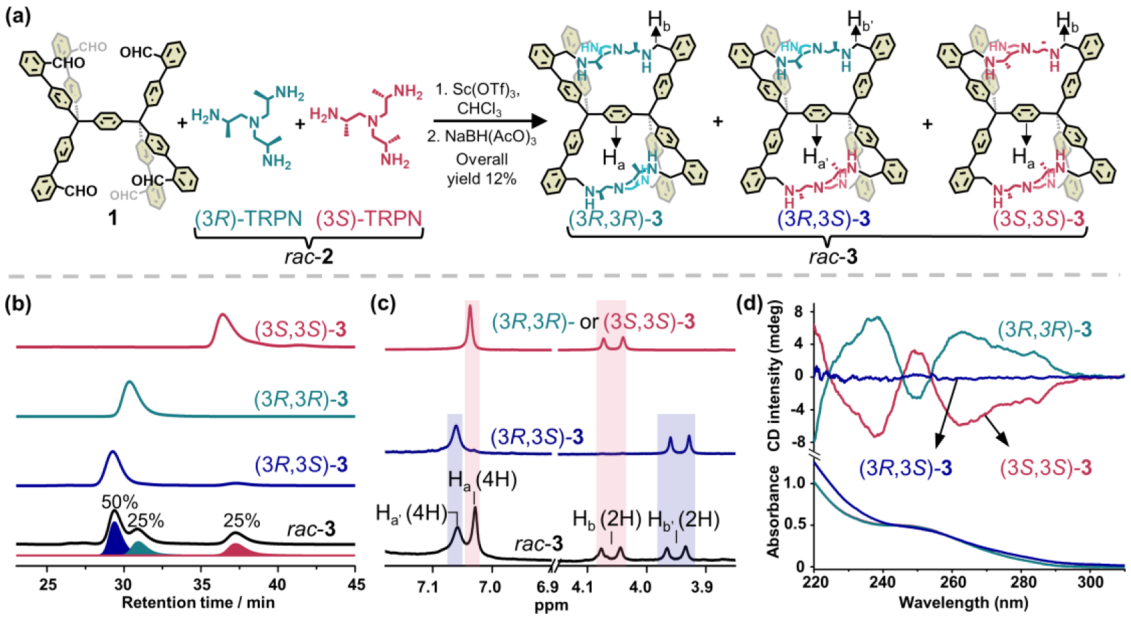

Figure 2. (a) Cycloimination of nonchiral hexa-aldehyde **1** with racemic triamine *rac*-**2** containing equal amount of (3*R*)- and (3*S*)-TRPN, followed by the reduction with $NaBH(AcO)_3$, yielding *rac*-**3** containing three *diphanes* (3*R*,3*R*)-**3** (25%), (3*R*,3*S*)-**3** (50%), and (3*S*,3*S*)-**3** (25%) in an overall yield of 12%. (b) Chiral HPLC chromatograms of (3*S*,3*S*)-**3** (magenta curve), (3*R*,3*R*)-**3** (cyan curve), (3*R*,3*S*)-**3** (blue curve), and *rac*-**3** (black curve). (c) ^{1}H NMR spectra (CD_2Cl_2, 400 MHz, 298 K) of (3*R*,3*R*)- or (3*S*,3*S*)-**3** (magenta curve), (3*R*,3*S*)-**3** (blue curve), and *rac*-**3** (black curve). (d) Electronic circular dichroism (top) and UV−vis absorption spectra (bottom) of (3*S*,3*S*)-**3** (magenta curve), (3*R*,3*R*)-**3** (cyan curve) and (3*R*,3*S*)-**3** (blue curve).

RESULTS AND DISCUSSION

Diastereomeric Discrimination of Heterochiral TRPN during *Diphane* Formation

We first attempted the cycloimination reaction between nonchiral hexa-aldehyde precursor **1** and racemic mixture *rac*-**2** composed of a pair of (*R*,*R*,*R*)- and (*S*,*S*,*S*)-TRPN (denoted (3*R*)- and (3*S*)-TRPN, Figure 2a). The matrix-assisted laser desorption ionization-time of flight mass spectrometry (MALDI-TOF MS) of the crude reaction mixture showed a major ion peak at *m*/*z* 1456.587, which corresponds to the expected *diphane* with the formula $C_{104}H_{95}N_8^+$ ($[M + H]^+$ calcd for 1456.771, Figure S16) for *rac*-**3**′ in the imine form. *Diphane rac*-**3**′ was further reduced

https://doi.org/10.1021/jacsau.2c00225
JACS Au 2022, 2, 1661−1668

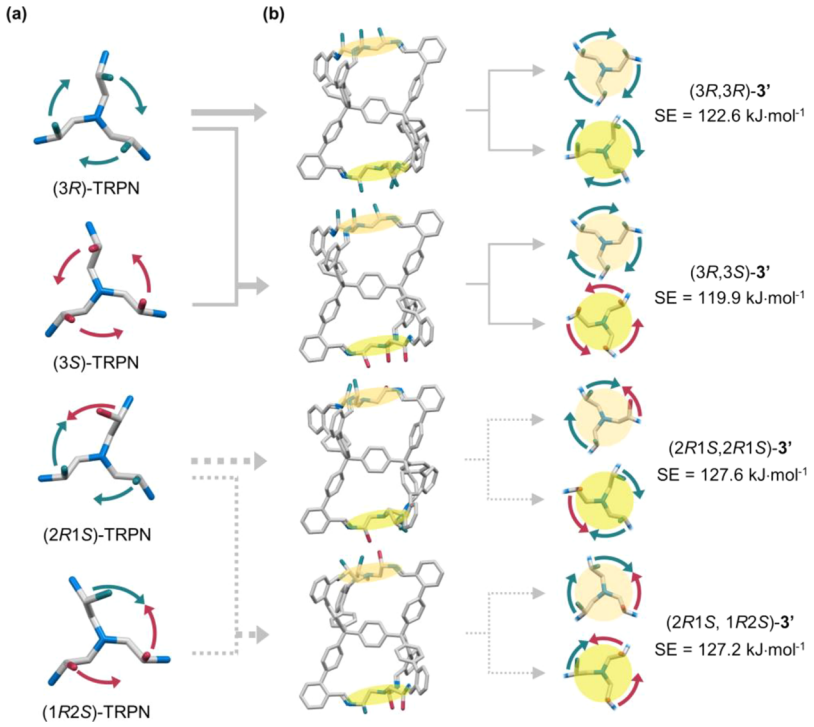

Figure 3. DFT calculations and inspection of structural effect of *rac*-**2** and *hetero*-**2** on the formation of *diphanes* in the imine form (denoted (3*R*,3*R*)-**3′** for example). (a) DFT calculations reveal that homochiral enantiomers (3*R*)- and (3*S*)-TRPN adopt regular orientations, whereas heterochiral (2*R*1*S*)- and (1*R*2*S*)-TRPN prefer disordered orientations. (b) Comparison of strain energy (SE) of homochiral *diphane* (3*R*,3*R*)-**3′**, achiral mesomer (3*R*,3*S*)-**3′**, and two virtual products, namely, heterochiral (2*R*1*S*,2*R*1*S*)-3′ and (2*R*1*S*,1*R*2*S*)-3′. The spatial orientations of the TRPN-derived moieties dissected from the corresponding (virtual) *diphanes* are given on the right side for comparison. Amines are in blue color. Hydrogen atoms are omitted for clarity.

with $NaBH(AcO)_3$, which yielded *rac*-**3** in the amine form so as to facilitate the product purification. The careful characterization of *rac*-**3** will be discussed in the next session (Figure 2). On the other hand, the reaction between precursor **1** and heterochiral TRPN was unable to yield any cage entity. This scenario was exemplified with *hetero*-**2** containing equal amount of epimers (2*R*1*S*)- and (1*R*2*S*)-TRPN (Figure S4). Out of 21 possible isomeric *diphanes* (Figure S7), none was formed with *hetero*-**2**, as they were even undetectable by MALDI-TOF MS (Figures S18 and S19).

This striking difference is that during the formation of a cage-like entity with a three-dimensional skeleton, nonchiral hexa-aldehyde **1** obviously prefers the homochiral to heterochiral isomers, although the reaction with the latter cannot be excluded in the resulting oligomers with an ill-defined structure. Taking (3*R*)-TRPN (one enantiomer in *rac*-**2**) and (2*R*1*S*)-TRPN (one epimer in *hetero*-**2**) for comparison, their different spatial orientation can be revealed by density functional theory (DFT with geometry optimization, M06-2X/6-31G*, Figure 3a). The three aliphatic chains of (3*R*)-TRPN all rotate anticlockwise, with three secondary amines being positioned in the same way; while the three aliphatic chains of (2*R*1*S*)-**2** are arranged in an uneven fashion, as one secondary amine rotates to the opposite direction of the other two.

We reasoned that the spatial orientation of these reactive amines might dramatically alter the formation possibility of *diphanes*. This hypothesis was probed by the comparison of SE of the *diphanes* (or virtual products) in the imine form (Figure 3b).[7b] DFT calculations show that (3*R*,3*R*)-**3′** exhibits a similar strain to that of mesomer (3*R*,3*S*)-**3′** (122.6 *vs* 119.9 kJ mol^{-1}). This strain is lower than those of virtual *diphanes* formed with heterochiral precursors, with the representative examples of (2*R*1*S*,2*R*1*S*)-**3′** with SE = 127.6 kJ mol^{-1} and (2*R*1*S*,1*R*2*S*)-**3′** with SE = 127.2 kJ mol^{-1}. Together with the experimental evidence, this significantly different SE therefore precludes the reaction with heterochiral TRPN during the formation of *diphanes*.

Formation of Homochiral and Achiral *Meso Diphanes*

As mentioned above, the condensation between precursor **1** with *rac*-**2** successfully yielded *diphane* in the imine form, which was then converted to the corresponding *rac*-**3** in the amine form to facilitate product purification (Figure 2a). We successfully resolved *rac*-**3** by chiral HPLC, which consists of three isomeric fractions in a 1:1:2 ratio (Figure 2b), respectively assigned to a pair of homochiral (3*R*,3*R*)-**3** and (3*S*,3*S*)-**3**, and an achiral mesomer (3*R*,3*S*)-**3** with reference compounds synthesized beforehand (Figures S5 and S6). In the ^1H NMR spectrum of *rac*-**3**, the sharp singlet at δ = 7.03 ppm and the doublet at δ = 4.06 ppm refer to homochiral *diphane* (3*R*,3*R*)-**3** or (3*S*,3*S*)-**3**, while the broad peak at δ = 7.06 ppm and the doublet at δ = 3.95 ppm correspond to the mesomer (3*R*,3*S*)-**3** (lower panel in Figure 2c, see assignment in Figure S64). This product distribution in *rac*-**3** is in accordance with DFT calculations, which showed little SE difference between the *diphanes* in the imine form (Figure 3, vide supra).

Electronic CD spectra of the three *diphanes* in tetrahydrofuran (THF) solutions were recorded (Figure 2d). Owing to similar structures, they share almost identical UV−vis absorption spectra. They all display a featureless absorption peak at *ca.* 250 nm, which is assigned to the $\pi \rightarrow \pi^*$ transitions

https://doi.org/10.1021/jacsau.2c00225
JACS Au 2022, 2, 1661−1668

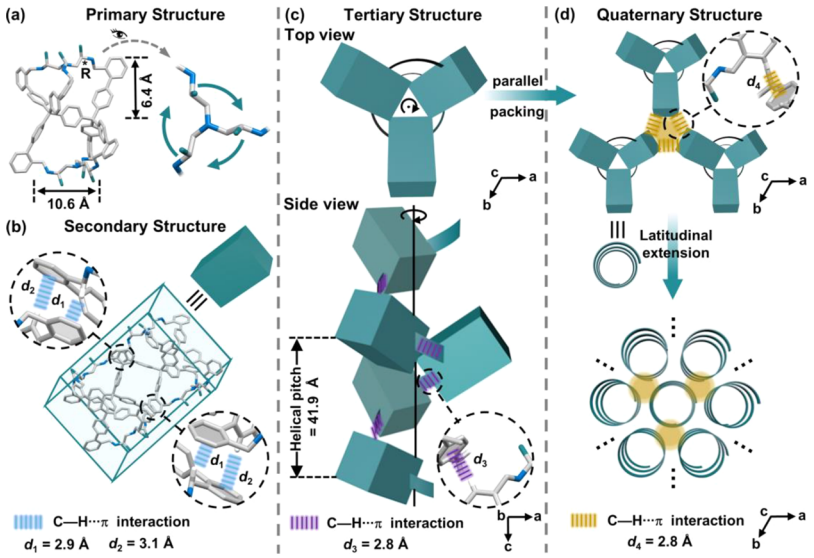

Figure 4. Hierarchical self-assembly of homochiral (3*R*,3*R*)-**3** molecules into the 3D acentric crystalline phase (trigonal space group $P3_221$). (a) Stick model of the primary structure (3*R*,3*R*)-**3** (left) and its top view (right) with three cyan arrows indicating the clockwise rotation of three aliphatic chains of TRPN-derived moiety. (b) Supramolecular dimer (secondary structure) self-assembled by (3*R*,3*R*)-**3** molecules via C−H···π interactions, simplified with a cuboid model. (c) Top view (top) and side view (bottom) of 3_2-helix (tertiary structure) with a helical pitch of 41.9 Å, self-organized by the cuboids (secondary structure) rotating by 120° via C−H···π interactions. (d) Latitudinal packing of the helices yields the trigonal crystalline phase (quaternary structure). Three helical columns are interconnected via C−H···π interactions.

of the twisted arenes in the cage skeleton. Obviously, *meso diphane* (3*R*,3*S*)-**3** is CD-silent due to the presence of the inversion center, while the two homochiral *diphanes* exhibit a mirror-image profile over the range between 220 and 300 nm, as expected for the enantiomeric pair.

Diphane (3*R*,3*R*)-**3** displays a positive cotton effect at 263 nm, followed by a negative one at 250 nm. This bisignate CD curve from longer to shorter wavelength (300−245 nm) is assigned to the *P*-configuration of three biphenyl arms of each propeller-like cavity. Similarly, the negative-to-positive bisignate curve is attributed to the *M*-configuration of *diphane* (3*S*,3*S*)-**3**. As compared to the previously reported single-cavity cages,[10,11] the value for the anisotropy factor of two chiral *diphanes* is relatively low (g_{abs} = 0.0004 at 240 nm). This low value probably results from the relatively higher symmetry of the upper and lower halves of the *diphanes* (Figure 4a, vide infra).

3D Hierarchical Structures Self-Assembled by Homochiral and *Meso Diphanes*

We[9b,12b,c] and other groups[8b,10b,12a,d,e] have demonstrated that cage-like compounds could serve as promising self-assembling tectons for the search of novel supramolecular materials. As part of our continuous endeavor, we investigated the self-assembly behavior of homochiral and achiral *meso diphanes* in their crystalline phases. We were particularly interested in the effect of configurational change on the resulting hierarchical superstructures.

Single crystals of two homochiral *diphanes* suitable for XRD were obtained by gradual evaporation of the solvent from their solutions in THF/CH_3CN = 1:4 (v/v) at a concentration of 15 mg/mL. *Diphanes* (3*R*,3*R*)-**3** and (3*S*,3*S*)-**3** crystallized into chiral superstructures of trigonal space group $P3_221$ and $P3_121$, respectively. We use (3*R*,3*R*)-**3** to represent homochiral *diphane* in the following discussion, and the structural analysis of (3*S*,3*S*)-**3** is given in Figures S12 and S13.

Its crystallographic analysis confirms the proposed structure of (3*R*,3*R*)-**3** with two identical cavities (Figures 4a and S9). Each cavity exhibits a diameter of 10.6 Å and a height of 6.4 Å. From the top view of a *diphane*, three aliphatic chains of each cavity adopt a clockwise rotation (cyan arrows, Figure 4a), which also holds true for the three methyl groups at the *R*-stereogenic centers. This clockwise rotation also induces the *P*-configuration of three biphenyl arms surrounding each cavity, in line with its CD spectrum (Figure 2d, vide supra).

Careful inspection of molecular packing of the homochiral *diphanes* reveals that each crystalline phase is a hierarchical superstructure, which share the similarity with those formed by biomacromolecules, block copolymers, and dendimers.[13] Serving as the primary structure, two (3*R*,3*R*)-**3** molecules self-assemble into a supramolecular dimer (secondary structure), simplified with a cuboid model, where the two adjacent *diphanes* are packed via quadruple C−H···π interactions (with d_1 = 2.9 Å and d_2 = 3.1 Å, Figures 4b and S10).

These dimers are arranged off crystallographic *c*-axis, around which a dimer rotates by 120° with respect to another, forming a single-handed 3_2-helix (tertiary structure) with a pitch of 41.9 Å (Figure 4c). Besides, along the helix, each *diphane* in the dimer below is packed with another *diphane* in the dimer above via C−H···π interaction with a distance of 2.8 Å (Figure 4c and S10). One helix is consequently packed in parallel with six neighboring helices via a network of C−H···π interactions (d_4 = 2.8 Å), as presented with the simplified spring-like model (Figures 4d and S11). This hierarchical self-assembly thus yields an acentric trigonal crystalline phase (quaternary structure), which is composed of an array of left-handed helices.[6c,6,14]

The superstructure of achiral (3*R*,3*S*)-**3** was also examined by XRD analysis of the single crystals obtained via slow evaporation of its solution in $CHCl_3$/CH_3OH = 1:4 (v/v) at a concentration of 15 mg/mL. (3*R*,3*S*)-**3** molecules instead crystallized into centrosymmetric crystalline phase of triclinic

https://doi.org/10.1021/jacsau.2c00225
JACS Au 2022, 2, 1661−1668

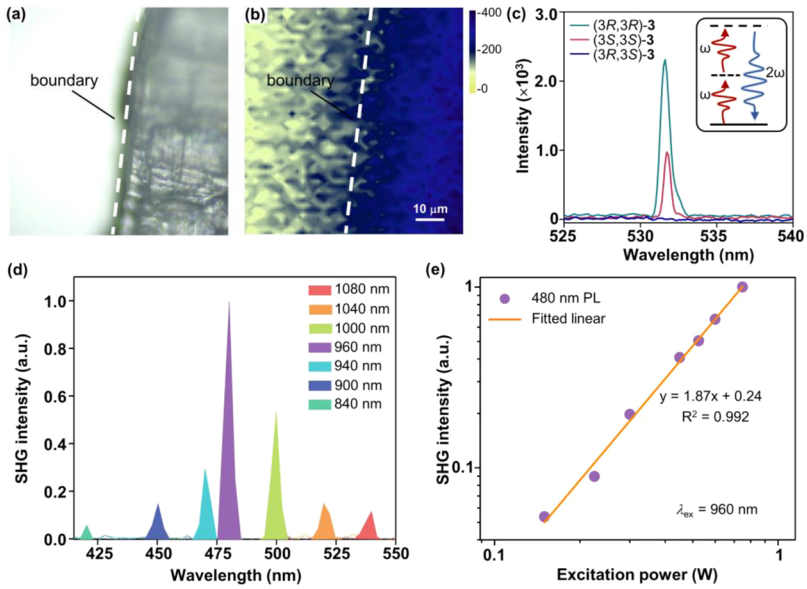

Figure 5. Different second-order nonlinear optical properties of three *diphane* crystals. (a) Optical and (b) SHG mapping images (λ_{ex} = 1064 nm) of (3*R*,3*R*)-**3** crystal within an 80 × 80 μm region. (c) SHG signal (532 nm) of (3*R*,3*R*)-**3**, (3*R*,3*S*)-**3**, and (3*S*,3*S*)-**3** single crystals under excitation with a 1064 nm laser (Inset: illustration of fundamental principle of SHG). (d) SHG intensities of (3*R*,3*R*)-**3** excited at various wavelengths from 840 to 1080 nm, represented with different colors. (e) Excitation power dependence of the SHG intensity at 480 nm (λ_{ex} = 960 nm) for (3*R*,3*R*)-**3** single crystals, with both axes shown on a logarithmic (log) scale. The fitted linear line satisfies the function $y = 1.87x + 0.24$, where y = lg[SHG intensity] and x = lg[excitation power]), and the fitted slope of ca. 2 confirms a typical second-order NLO process.

space group $P\bar{1}$. The detailed structural analysis of this superstructure is illustrated in Figure S14.

NLO Properties of Hierarchical Superstructures Self-Assembled by Homochiral and Achiral *Meso Diphanes*

As mentioned above, *diphanes* (3*S*,3*S*)-/(3*R*,3*R*)-**3** and (3*R*,3*S*)-**3** respectively self-assemble into acentric and centrosymmetric superstructures, which may endow them with different properties and functions. As a proof of concept, we explored their quadratic NLO effect, namely, SHG activity. In a typical SHG process, as mediated by the transition through a virtual energy state, two incident photons with frequency ω interact within an acentric medium, which subsequently are converted into an emitted photon with a doubled frequency 2ω (inset in Figure 5c). Compared to conventional inorganic dielectrics and semiconductors, organic NLO counterparts exhibit advantages such as light weight, large nonlinear coefficient, and flexibility,[15] which thus hold promise for the application in soft photo-electronics and photonics.

We first irradiated the single crystals of *diphanes* (3*S*,3*S*)-**3**, (3*R*,3*R*)-**3**, and (3*R*,3*S*)-**3** with a Nd-yttrium-aluminum-garnet (Nd:YAG) laser beam (1064 nm, 20 Hz, 8 ns) at an angle of 45°. As shown with partial optical (Figure 5a) and SHG mapping (Figure 5b) images of a (3*R*,3*R*)-**3** single crystal, for example, it exhibits a clear SHG response at 532 nm (right side of the dashed line), which is only active for the non-centrosymmetric crystalline phase. This is evident when compared with the substrate on which the crystal is deposited (left side of the dashed line, Figure 5b), where negligible output was observed. On the other hand, no SHG signal was detected for the centrosymmetric crystalline phase of achiral (3*R*,3*S*)-**3** (Figure S15c). When the SHG response of the three *diphanes* was recorded in the transmission direction, the difference is unambiguous, as both homochiral (3*S*,3*S*)-**3** and (3*R*,3*R*)-**3** display strong and sharp peaks, while that of (3*R*,3*S*)-**3** is near zero (Figure 5b). It is worth noting that we intentionally selected different sizes of single crystals of the two *diphanes*, so as to avoid the overlap of their SHG intensity.[16]

To further explore the NLO property of the superstructures formed by homochiral *diphanes*, at a fixed pumping power, the wavelength-dependent SHG behavior[15b,16] of a (3*R*,3*R*)-**3** single crystal was investigated with different wavelengths (λ_{ex} = 840−1080 nm, Figure 5d). It shows that the intensity of optical signals indeed varies with wavelength, with the highest photoluminescence intensity under excitation at λ_{ex} = 960 nm. Moreover, both the fitted linear relationship between SHG intensity (λ_{em} = 480 nm) and excitation power (W, λ_{ex} = 960 nm) on a logarithmic scale also reveals a typical second-order NLO behavior (Figure 5e).

CONCLUSIONS

In summary, we showed that among heterochiral and homochiral TRPN diastereomers, only the enantiomeric pair of homochiral isomers were selected by nonchiral hexa-aldehyde precursor **1** via cycloimination, forming the corresponding homochiral cages with twin-cavity (denoted (3*R*,3*R*)-/(3*S*,3*S*)-*diphane*) and their mesomer (3*R*,3*S*)-*diphane*. As revealed by DFT calculations, this discrimination of heterochiral isomers results from the different spatial orientation of reactive amines of TRPN. This example is distinct from the previous findings showing a similar reactivity of diastereomeric synthons under DCC conditions.[17]

We also showed that the self-assembly of homo- and achiral *diphanes* is dramatically different. The former forms an array of single-handed supramolecular helices with interesting second-order NLO properties, while the latter self-assembles into the centrosymmetric supramolecular columnar phase. Different from the current research focus of organic cages on their design, synthesis, and host−guest utility of their porosity,[8] our study showcases their promise with a tailored shape and structure for the search of a novel hierarchical superstructure

https://doi.org/10.1021/jacsau.2c00225
JACS Au 2022, 2, 1661−1668

with emergent properties and functions, which include but are not limited to nonlinear optics, bulk photovoltaics, and organic ferroelectrics. These topics are currently ongoing in our laboratories, which will be reported in due course.

METHODS

Materials

Dimethyl terephthalate, phenyl lithium, aniline, tetrakis-(triphenylphosphine)palladium, scandium(III) trifluorometha-nesulfonate, and phenol were purchased from Beijing J&K Chemical Co. Ltd. 2-Formylbenzeneboronic acid, (*rac*)-alaninol, (*S*)-alaninol, (*R*)-alaninol, and *p*-toluene sulfonyl chloride were purchased from Beijing InnoChem Co. Ltd. Sodium triacetoxyborohydride was purchased from Shanghai Adamas-Beta Co. Ltd. Inorganic salts including sodium nitrite, potassium carbonate, and potassium hydroxide were purchased from Greagent, China. THF was dried over sodium/benzophenone and distilled under a nitrogen atmosphere before use.

General Instrumentation

Nuclear magnetic resonance (NMR) spectra were performed on a Bruker Avance III HD 400 spectrometer at room temperature. MALDI-TOF MS was performed on a solariX XR 7.0 T hybrid quadrupole−FT ICR mass spectrometer (Bruker Daltonics, Bremen, Germany), using an ESI/APCI/MALDI ion source and external ion accumulation in positive ion mode. SC-XRD data were collected on a Bruker D8 Venture diffractometer. CD spectra were recorded on a Jasco J-1500 spectrometer at 25 °C. Analytical HPLC was conducted on a Shimadzu LC-20 AD system at 30 °C. The SHG measurement was conducted using a titanium−sapphire pulsed laser (Coherent, 140 fs pulse width, 80 MHz repetition rate).

Synthesis of *Diphane Rac*-3, (3*S*,3*S*)-3, (3*R*,3*R*)-3, and (3*R*,3*S*)-3

***Rac*-3.** A 0.005 mol/L solution of hexa-aldehyde molecule **1** (200.0 mg, 0.168 mmol, 1 equiv) in 33.7 mL $CHCl_3$ was charged into a 250 mL flask. Then a 0.005 mol/L solution of *rac*-**2** (63.5 mg, 0.336 mmol, 2.0 equiv) in 67.5 mL $CHCl_3$ was added dropwise, followed by addition of $Sc(OTf)_3$ (50 mg, 0.10 mmol, 0.6 equiv) directly. The reaction mixture was stirred at 25 °C for 24 h. Then, the product was reduced by $NaBH(OAc)_3$ (0.54 g, 2.53 mmol, 15.0 equiv) overnight, the excess reductant $NaBH(OAc)_3$ was filtered off under vacuum, and the solution was quenched with NaOH solution (2.0 M, 120 mL), extracted with $CHCl_3$ (3 × 50 mL), dried over anhydrous Na_2SO_4, and concentrated to give the crude product. Purification by flash column chromatography (DCM/MeOH/NH_3(aq) = 150:2:3, v/v/v) afforded the *diphane rac*-**3** (30 mg, 12%) as a white solid. HR-MS (MALDI): before reduction: $C_{104}H_{95}N_8^+$ $[M + H]^+$, calcd: 1456.771; Found: 1456.587; after reduction: $C_{104}H_{107}N_8^+$ $[M + H]^+$, calcd: 1468.865; Found: 1468.714.

(3*S*,3*S*)-3. A 0.005 mol/L solution of hexa-aldehyde molecule **1** (500.0 mg, 0.42 mmol, 1 equiv) in 84.3 mL $CHCl_3$ was charged into a 500 mL flask. Then a 0.005 mol/L solution of (3*S*)-TRPN (158.7 mg, 0.84 mmol, 2.0 equiv) in 168.6 mL $CHCl_3$ was added dropwise, followed by addition of $Sc(OTf)_3$ (124.4 mg, 0.25 mmol, 0.6 equiv). The reaction mixture was stirred at 25 °C for 24 h. Then, the product was reduced by $NaBH(OAc)_3$ (1.34 g, 6.32 mmol, 15.0 equiv) overnight, the excess reductant $NaBH(OAc)_3$ was filtered off under vacuum, and the solution was quenched with NaOH solution (2.0 M, 300 mL), extracted with $CHCl_3$ (3 × 150 mL), dried over anhydrous Na_2SO_4, and concentrated to give the crude product. Purification by flash column chromatography (DCM/MeOH/NH_3(aq) = 150:2:3, v/v/v) afforded the *diphane* (3*S*,3*S*)-**3** (68 mg, 11%) as a white solid. ^{1}H NMR (400 MHz, CD_2Cl_2, 298 K), δ = 7.05−7.57 (m, 52H), 4.07 (d, J = 12.0 Hz, 2H), 3.74 (d, J = 12.0 Hz, 2H), 3.62 (dd, J = 12.0 Hz, 12.0 Hz, 4H), 3.51 (d, J = 12.0 Hz, 2H), 3.37 (d, J = 12.0 Hz, 2H), 2.71−2.80 (m, 2H), 2.61−2.71 (m, 2H), 2.42−2.52 (m, 2H), 2.07−2.14 (m, 6H), 1.88−1.95 (m, 4H), 1.76 (d, J = 12.0 Hz, 2H), 1.13−1.19 (m, 18H). ^{13}C NMR (101 MHz, CD_2Cl_2, 298 K), δ = 145.97, 145.82, 145.41, 144.53, 142.47, 142.20, 141.27, 139.64, 139.49, 139.03, 138.96, 138.26, 131.36, 130.84, 130.10,130.00, 129.79, 129.07, 128.44, 128.36, 127.89, 127.81, 127.68, 127.62, 127.41, 64.13, 63.68, 62.40, 61.58, 52.63, 52.20, 51.80, 50.26, 49.09, 20.85, 20.44, 19.69. HR-MS (MALDI): $C_{104}H_{107}N_8^+$ $[M + H]^+$, calcd: 1468.865; Found: 1468.749.

(3*R*,3*R*)-**3** was obtained from hexa-aldehyde molecule **1** and (3*R*)-TRPN as starting materials, which was synthesized according the same procedure of (3*S*,3*S*)-**3**.

(3*R*,3*S*)-3. A 0.005 mol/L solution of intermediate compound **4** (57.5 mg, 0.043 mmol, 1 equiv) in 8.7 mL $CHCl_3$ was charged into a 25 mL flask. Then a 0.005 mol/L solution of (3*R*)-TRPN (8.2 mg, 0.043 mmol, 1.0 equiv) in 8.7 mL $CHCl_3$ was added dropwise, followed by addition of $Sc(OTf)_3$ (6.4 mg, 0.013 mmol, 0.3 equiv). The reaction mixture was stirred at 25 °C for 24 h. Then, the product was reduced by $NaBH(OAc)_3$ (68.8 mg, 0.32 mmol, 7.5 equiv) overnight, the excess reductant $NaBH(OAc)_3$ was filtered off under vacuum, and the solution was quenched with NaOH solution (2.0 M, 15 mL), extracted with $CHCl_3$ (3 × 20 mL), dried over anhydrous Na_2SO_4, and concentrated to give the crude product. Purification by flash column chromatography (DCM/MeOH/NH_3(aq) = 150:2:3, v/v/v) afforded the (3*R*,3*S*)-**3** (40 mg, 63%) as a white solid. ^{1}H NMR (400 MHz, CD_2Cl_2, 298 K), δ = 7.06−7.50 (m, 52H), 3.95 (d, J = 12.0 Hz, 2H), 3.75 (d, J = 12.0 Hz, 2H), 3.65 (d, J = 12.0 Hz, 2H), 3.57 (d, J = 12.0 Hz, 2H), 3.52 (d, J = 12.0 Hz, 2H), 3.41 (d, J = 12.0 Hz, 2H), 2.62−2.78 (m, 4H), 2.43−2.52 (m, 2H), 1.87−2.07 (m, 10H), 1.57 (d, J = 12.0 Hz, 2H), 1.10−1.13 (m, 18H). ^{13}C NMR (101 MHz, CD_2Cl_2, 298 K), δ = 146.10, 145.90, 145.51, 144.67, 142.51, 141.98, 139.96, 139.51, 139.46, 137.26, 131.80, 131.00, 130.45, 130.28, 130.04, 129.92, 129.48, 128.98, 128.51, 128.24, 128.11, 127.97, 127.89, 127.80, 127.39, 64.33, 62.75, 61.92, 61.17, 52.98, 52.13, 52.05, 51.65, 20.25, 19.57, 18.73. HR-MS (MALDI): $C_{104}H_{107}N_8^+$ $[M + H]^+$, calcd: 1468.865; Found: 1468.863.

ASSOCIATED CONTENT

Supporting Information

The Supporting Information is available free of charge at https://pubs.acs.org/doi/10.1021/jacsau.2c00225.

Characterization methods, experimental details, theoretical calculation details, and characterization of compounds (PDF)

AUTHOR INFORMATION

Corresponding Author

Shaodong Zhang − *School of Chemistry and Chemical Engineering, Shanghai Jiao Tong University, Shanghai 200240, China;* orcid.org/0000-0001-7923-8457; Email: sdzhang@sjtu.edu.cn

Authors

Jiaolong Chen − *School of Chemistry and Chemical Engineering, Shanghai Jiao Tong University, Shanghai 200240, China*

Zhenyu Yang − *School of Chemistry and Chemical Engineering, Shanghai Jiao Tong University, Shanghai 200240, China*

Gucheng Zhu − *Key Laboratory of Artificial Structures and Quantum Control (Ministry of Education), Shenyang National Laboratory for Materials Science, School of Physics and Astronomy, Shanghai Jiao Tong University, Shanghai 200240, China*

Enguang Fu − *School of Chemistry and Chemical Engineering, Shanghai Jiao Tong University, Shanghai 200240, China*

Pan Li − *School of Chemistry and Chemical Engineering, Shanghai Jiao Tong University, Shanghai 200240, China*

Fangyi Chen − *School of Chemistry and Chemical Engineering, Shanghai Jiao Tong University, Shanghai 200240, China*

Chunyang Yu − *School of Chemistry and Chemical Engineering, Shanghai Jiao Tong University, Shanghai 200240, China;* orcid.org/0000-0003-1175-8362

Shiyong Wang − *Key Laboratory of Artificial Structures and Quantum Control (Ministry of Education), Shenyang National Laboratory for Materials Science, School of Physics and Astronomy, Shanghai Jiao Tong University, Shanghai 200240, China;* orcid.org/0000-0001-6603-9926

Complete contact information is available at: https://pubs.acs.org/10.1021/jacsau.2c00225

Notes

The authors declare no competing financial interest.
Crystallographic data have been deposited with the Cambridge Crystallographic Data Centre as entries CCDC 2144436, 2144437 and 2144438

■ ACKNOWLEDGMENTS

The authors gratefully acknowledge financial support from Science and Technology Commission of Shanghai Municipality (21JC1401700) and National Natural Science Foundation of China (21890733 and 22071153). We appreciate the assistance from Dr. Hang Wang (MALDI-TOF MS) and Ling-Ling Li (SC-XRD) at the Instrumental Analysis Centre of SJTU. We also thank Prof. Yang Tian and Dr. Zhichao Liu from East China Normal University, Mr. Zhengfei Liu from Beijing Normal University for the help of nonlinear optical experiments.

■ REFERENCES

(1) (a) Barron, L. D. Chirality and Life. *Space Sci. Rev.* **2008**, *135*, 187−201. (b) Morrow, S. M.; Bissette, A. J.; Fletcher, S. P. Transmission of Chirality through Space and across Length Scales. *Nat. Nanotechnol.* **2017**, *12*, 410−419.

(2) (a) Feringa, B. L.; van Delden, R. A. Absolute Asymmetric Synthesis: The Origin, Control, and Amplification of Chirality. *Angew. Chem., Int. Ed.* **1999**, *38*, 3418−3438. (b) Blackmond, D. G. The Origin of Biological Homochirality. *Cold Spring Harbor Perspect. Biol.* **2010**, *2*, a002147.

(3) Pasteur, L. Mémoire sur la Relation Qui Peut Exister entre la Forme Cristalline et la Composition Chimique, et sur la Cause de la Polarisation Rotatoire. *C. R. Séances Acad. Sci.* **1848**, *26*, 535−538.

(4) (a) Tsuji, N.; Kennemur, J. L.; Buyck, T.; Lee, S.; Prévost, S.; Kaib, P. S. J.; Bykov, D.; Farès, C.; List, B. Activation of Olefins via Asymmetric Brønsted Acid Catalysis. *Science* **2018**, *359*, 1501−1505. (b) Shin, N. Y.; Ryss, J. M.; Zhang, X.; Miller, S. J.; Knowles, R. R. Light-Driven Deracemization Enabled by Excited-State Electron Transfer. *Science* **2019**, *366*, 364−369.

(5) (a) Ishida, Y.; Aida, T. Homochiral Supramolecular Polymerization of an "S"-Shaped Chiral Monomer: Translation of Optical Purity into Molecular Weight Distribution. *J. Am. Chem. Soc.* **2002**, *124*, 14017−14019. (b) Helmich, F.; Smulders, M. M. J.; Lee, C. C.; Schenning, A. P. H. J.; Meijer, E. W. Effect of Stereogenic Centers on the Self-Sorting, Depolymerization, and Atropisomerization Kinetics of Porphyrin-Based Aggregates. *J. Am. Chem. Soc.* **2011**, *133*, 12238−12246. (c) Roche, C.; Sun, H.-J.; Prendergast, M. E.; Leowanawat, P.; Partridge, B. E.; Heiney, P. A.; Araoka, F.; Graf, R.; Spiess, H. W.; Zeng, X.; Ungar, G.; Percec, V. Homochiral Columns Constructed by Chiral Self-Sorting During Supramolecular Helical Organization of Hat-Shaped Molecules. *J. Am. Chem. Soc.* **2014**, *136*, 7169−7185. (d) Hu, Y.; Teat, S. J.; Gong, W.; Zhou, Z.; Jin, Y.; Chen, H.; Wu, J.; Cui, Y.; Jiang, T.; Cheng, X.; Zhang, W. Single Crystals of Mechanically Entwined Helical Covalent Polymers. *Nat. Chem.* **2021**, *13*, 660−665. (e) Liu, M.; Zhang, L.; Wang, T. Supramolecular Chirality in Self-Assembled Systems. *Chem. Rev.* **2015**, *115*, 7304−7397.

(6) (a) Meng, W.; Ronson, T. K.; Nitschke, J. R. Symmetry Breaking in Self-Assembled M_4L_6 Cage Complexes. *Proc. Natl. Acad. Sci. U. S. A.* **2013**, *110*, 10531−10535. (b) Samanta, A.; Liu, Z.; Nalluri, S. K. M.; Zhang, Y.; Schatz, G. C.; Stoddart, J. F. Supramolecular Double-Helix Formation by Diastereoisomeric Conformations of Configurationally Enantiomeric Macrocycles. *J. Am. Chem. Soc.* **2016**, *138*, 14469−14480. (c) Roche, C.; Sun, H.-J.; Leowanawat, P.; Araoka, F.; Partridge, B. E.; Peterca, M.; Wilson, D. A.; Prendergast, M. E.; Heiney, P. A.; Graf, R.; Spiess, H. W.; Zeng, X.; Ungar, G.; Percec, V. A Supramolecular Helix that Disregards Chirality. *Nat. Chem.* **2016**, *8*, 80−88. (d) Ousaka, N.; Yamamoto, S.; Iida, H.; Iwata, T.; Ito, S.; Hijikata, Y.; Irle, S.; Yashima, E. Water-Mediated Deracemization of a Bisporphyrin Helicate Assisted by Diastereoselective Encapsulation of Chiral Guests. *Nat. Commun.* **2019**, *10*, 1457.

(7) (a) Greenaway, R. L.; Santolini, V.; Szczypinski, F. T.; Bennison, M. J.; Little, M. A.; Marsh, A.; Jelfs, K. E.; Cooper, A. I. Organic Cage Dumbbells. *Chem. − Eur. J.* **2020**, *26*, 3718−3722. (b) Wang, Y.; Zhang, Y.; Zhou, Z.; Vanderlinden, R. T.; Li, B.; Song, B.; Li, X.; Cui, L.; Li, J.; Jia, X.; Fang, J.; Li, C.; Stang, P. J. A Cyclic Bis[2]Catenane Metallacage. *Nat. Commun.* **2020**, *11*, 2727. (c) Cheng, P. M.; Cai, L. X.; Li, S. C.; Hu, S. J.; Yan, D. N.; Zhou, L. P.; Sun, Q. F. Guest-Reaction Driven Cage to Conjoined Twin-Cage Mitosis-Like Host Transformation. *Angew. Chem., Int. Ed.* **2020**, *59*, 23569−23573. (d) Yang, Z.; Yu, C.; Chen, L.; Li, P.; Chen, J.; Wu, K. J.; Zhu, Q.; Zhao, Y.-Q.; Liu, X.; Zhang, S. A Class of Organic Cages Featuring Twin Cavities. *Nat. Commun.* **2021**, *12*, 6124. (e) Cai, L.-X.; Yan, D.-N.; Cheng, P.-M.; Xuan, J.-J.; Li, S.-C.; Zhou, L.-P.; Tian, C.-B.; Sun, Q.-F. Controlled Self-Assembly and Multistimuli-Responsive Interconversions of Three Conjoined Twin-Cages. *J. Am. Chem. Soc.* **2021**, *143*, 2016−2024.

(8) (a) Jin, Y.; Voss, B. A.; Noble, R. D.; Zhang, W. A Shape-Persistent Organic Molecular Cage with High Selectivity for the Adsorption of CO_2 over N_2. *Angew. Chem., Int. Ed.* **2010**, *49*, 6348−6351. (b) Jones, J. T. A.; Holden, D.; Mitra, T.; Hasell, T.; Adams, D. J.; Jelfs, K. E.; Trewin, A.; Willock, D. J.; Day, G. M.; Bacsa, J.; Steiner, A.; Cooper, A. I. On−Off Porosity Switching in a Molecular Organic Solid. *Angew. Chem., Int. Ed.* **2011**, *50*, 749−753. (c) Avellaneda, A.; Valente, P.; Burgun, A.; Evans, J. D.; Markwell-Heys, A. W.; Rankine, D.; Nielsen, D. J.; Hill, M. R.; Sumby, C. J.; Doonan, C. J. Kinetically Controlled Porosity in a Robust Organic Cage Material. *Angew. Chem., Int. Ed.* **2013**, *52*, 3746−3749. (d) Bera, S.; Basu, A.; Tothadi, S.; Garai, B.; Banerjee, S.; Vanka, K.; Banerjee, R. Odd−Even Alternation in Tautomeric Porous Organic Cages with Exceptional Chemical Stability. *Angew. Chem., Int. Ed.* **2017**, *56*, 2123−2126. (e) Su, K.; Wang, W.; Du, S.; Ji, C.; Yuan, D. Efficient Ethylene Purification by a Robust Ethane-Trapping Porous Organic Cage. *Nat. Commun.* **2021**, *12*, 3703.

(9) (a) Beaudoin, D.; Rominger, F.; Mastalerz, M. Chiral Self-Sorting of [2+3] Salicylimine Cage Compounds. *Angew. Chem., Int. Ed.* **2017**, *56*, 1244−1248. (b) Sun, Z.; Li, P.; Xu, S.; Li, Z.-Y.; Nomura, Y.; Li, Z.-M.; Liu, X.; Zhang, S. Controlled Hierarchical Self-Assembly of Catenated Cages. *J. Am. Chem. Soc.* **2020**, *142*, 10833−10840. (c) Li, P.; Sun, Z.; Chen, J.; Zuo, Y.; Yu, C.; Liu, X.; Yang, Z.; Chen, L.; Fu, E.; Wang, W.; Liu, Z.; Hu, J.; Zhang, S. Spontaneous Resolution of Racemic Cage-Catenanes via Sequential Diastereomeric Enrichment and Supramolecular Narcissistic Self-Sorting. *J. Am. Chem. Soc.* **2022**, *144*, 1342−1350.

(10) (a) Qu, H.; Wang, Y.; Li, Z.; Wang, X.; Fang, H.; Tian, Z.; Cao, X. Molecular Face-Rotating Cube with Emergent Chiral and Fluorescence Properties. *J. Am. Chem. Soc.* **2017**, *139*, 18142−18145. (b) Wagner, P.; Rominger, F.; Zhang, W.-S.; Gross, J. H.; Elbert, S. M.; Schrçder, R. R.; Mastalerz, M. Chiral Self-Sorting of Giant Cubic [8+12] Salicylimine Cage Compounds. *Angew. Chem., Int. Ed.* **2021**, *60*, 8896−8904. (c) Li, C.; Zuo, Y.; Zhao, Y.-Q.; Zhang,

S. Chiral Self-Sorting in Cage-like Compounds. *Chem. Lett.* **2020**, *49*, 28−53.
(11) (a) Xu, D.; Warmuth, R. Edge-Directed Dynamic Covalent Synthesis of a Chiral Nanocube. *J. Am. Chem. Soc.* **2008**, *130*, 7520−7521. (b) Wang, X.; Wang, Y.; Yang, H.; Fang, H.; Chen, R.; Sun, Y.; Zheng, N.; Tan, K.; Lu, X.; Tian, Z.; Cao, X. Assembled Molecular Face-Rotating Polyhedra to Transfer Chirality from Two to Three Dimensions. *Nat. Commun.* **2016**, *7*, 12469. (c) Chen, Y.; Wu, G.; Chen, B.; Qu, H.; Jiao, T.; Li, Y.; Ge, C.; Zhang, C.; Liang, L.; Zeng, X.; Cao, X.; Wang, Q.; Li, H. Self-Assembly of a Purely Covalent Cage with Homochirality by Imine Formation in Water. *Angew. Chem., Int. Ed.* **2021**, *60*, 18815−18820.
(12) (a) Zhang, C.; Patil, R. S.; Liu, C.; Barnes, C. L.; Atwood, J. L. Controlled 2D Assembly of Nickel-Seamed Hexameric Pyro-gallol[4]-arene Nanocapsules. *J. Am. Chem. Soc.* **2017**, *139*, 2920−2923. (b) Liu, X.; Zhu, G.; He, D.; Gu, L.; Shen, P.; Cui, G.; Wang, S.; Shi, Z.; Miyajima, D.; Wang, S.; Zhang, S. Guest Mediated Hierarchical Self-Assembly of Dissymmetric Organic Cages to Form Supramolecular Ferroelectrics. *CCS Chem.* **2021**, *3*, 2473−2481. (c) Liu, X.; Shi, Z.; Xie, M.; Xu, J.; Zhou, Z.; Jung, S.; Cui, G.; Li, T.; Liu, Z.; Zhang, S. Single-Handed Double Helix and Spiral Platelet Formed by Racemate of Dissymmetric Cages. *Angew. Chem., Int. Ed.* **2021**, *60*, 15080−15086. (d) Wang, H.; Wang, K.; Xu, Y.; Wang, W.; Chen, S.; Hart, M.; Wojtas, L.; Zhou, L.-P.; Gan, L.; Yan, X.; Li, Y.; Lee, J.; Ke, X.-S.; Wang, X.-Q.; Zhang, C.-W.; Zhou, S.; Zhai, T.; Yang, H.-B.; Wang, M.; He, J.; Sun, Q.-F.; Xu, B.; Jiao, Y.; Stang, P. J.; Sessler, J. L.; Li, X. Hierarchical Self-Assembly of Nanowires on the Surface by Metallo-Supramolecular Truncated Cuboctahedra. *J. Am. Chem. Soc.* **2021**, *143*, 5826−5835. (e) Wang, H.; Zhou, L.-P.; Zheng, Y.; Wang, K.; Song, B.; Yan, X.; Wojtas, L.; Wang, X.-Q.; Jiang, X.; Wang, M.; Sun, Q.-F.; Xu, B.; Yang, H.-B.; Sue, A. C.-H.; Chan, Y.-T.; Sessler, J. L.; Jiao, Y.; Stang, P. J.; Li, X. Double-Layered Supramolecular Prisms Self-Assembled by Geometrically Non-Equivalent Tetratopic Subunits. *Angew. Chem., Int. Ed.* **2021**, *60*, 1298−1305.
(13) (a) Linderstrøm-Lang, K. U. *Lane Medical Lectures: Proteins and Enzymes*; Stanford Univ. Publ. Med. Series, 1952; Vol. *6*, pp 1−115. (b) Rosen, B. M.; Wilson, C. J.; Wilson, D. A.; Peterca, M.; Imam, M. R.; Percec, V. Dendron-Mediated Self-Assembly, Disassembly, and Self-Organization of Complex Systems. *Chem. Rev.* **2009**, *109*, 6275−6540. (b) Huang, M.; Hsu, C.-H.; Wang, J.; Mei, S.; Dong, X.; Li, Y.; Li, M.; Liu, H.; Zhang, W.; Aida, T.; Zhang, W.-B.; Yue, K.; Cheng, S. Z. D. Selective Assemblies of Giant Tetrahedra via Precisely Controlled Positional Interactions. *Science* **2015**, *348*, 424−428. (c) Kim, K.; Schulze, M. W.; Arora, A.; Lewis, R. M.; Hillmyer, M. A.; Dorfman, K. D.; Bates, F. S. Thermal Processing of Diblockcopolymer Melts Mimics Metallurgy. *Science* **2017**, *356*, 520−523. (d) Wang, L.; Partridge, B. E.; Huang, N.; Olsen, J. T.; Sahoo, D.; Zeng, X.; Ungar, G.; Graf, R.; Spiess, H. W.; Percec, V. Extraordinary Acceleration of Cogwheel Helical Self-Organization of Dendronized Perylene Bisimides by the Dendron Sequence Encoding Their Tertiary Structure. *J. Am. Chem. Soc.* **2020**, *142*, 9525−9536.
(14) (a) Bae, J.; Choi, J.-H.; Yoo, Y.-S.; Oh, N.-K.; Kim, B.-S.; Lee, M. Helical Nanofibers from Aqueous Self-Assembly of an Oligo(*p*-phenylene)-Based Molecular Dumbbell. *J. Am. Chem. Soc.* **2005**, *127*, 9668−9669. (b) Greenfield, J. L.; Evans, E. W.; Di Nuzzo, D.; Di Antonio, M.; Friend, R. H.; Nitschke, J. R. Unraveling Mechanisms of Chiral Induction in Double-Helical Metallopolymers. *J. Am. Chem. Soc.* **2018**, *140*, 10344−10353. (c) Yashima, E.; Ousaka, N.; Taura, D.; Shimomura, K.; Ikai, T.; Maeda, K. Supramolecular Helical Systems: Helical Assemblies of Small Molecules, Foldamers, and Polymers with Chiral Amplification and Their Functions. *Chem. Rev.* **2016**, *116*, 13752−13990.
(15) (a) Verbiest, T.; Elshocht, S. V.; Kauranen, M.; Hellemans, L.; Snauwaert, J.; Nuckolls, C.; Katz, T. J.; Persoons, A. Strong Enhancement of Nonlinear Optical Properties Through Supramolecular Chirality. *Science* **1998**, *282*, 913−915. (b) Zhu, W.; Zhu, L.; Sun, L.; Zhen, Y.; Dong, H.; Wei, Z.; Hu, W. Uncovering the Intramolecular Emission and Tuning the Nonlinear Optical Properties of Organic Materials by Cocrystallization. *Angew. Chem., Int. Ed.* **2016**, *55*, 14023−14027. (c) Lou, A. J.-T.; Righetto, S.; Barger, C.; Zuccaccia, C.; Cariati, E.; Macchioni, A.; Marks, T. J. Unprecedented Large Hyperpolarizability of Twisted Chromophores in Polar Media. *J. Am. Chem. Soc.* **2018**, *140*, 8746−8755.
(16) Ok, K. M.; Chi, E. O.; Halasyamani, P. S. Bulk Characterization Methods for Non-Centrosymmetric Materials: Second-Harmonic Generation, Piezoelectricity, Pyroelectricity, and Ferroelectricity. *Chem. Soc. Rev.* **2006**, *35*, 710−717.
(17) (a) Corbett, P. T.; Tong, H. L.; Sanders, J. K. M.; Otto, S. Diastereoselective Amplification of an Induced-Fit Receptor from a Dynamic Combinatorial Library. *J. Am. Chem. Soc.* **2005**, *127*, 8902−8903. (b) Chung, M.-K.; Hebling, C. M.; Jorgenson, J. W.; Severin, K.; Lee, S. J.; Gagné, M. R. Deracemization of a Dynamic Combinatorial Library Induced by (−)-Cytidine and (−)-2-Thiocytidine. *J. Am. Chem. Soc.* **2008**, *130*, 11819−11827. (c) Chung, M.-K.; Severin, K.; Lee, S. J.; Waters, M. L.; Gagné, M. R. Constitutionally Selective Amplification of Multicomponent 84-Membered Macrocyclic Hosts for (−)-cytidine•H^+. *Chem. Sci.* **2011**, *2*, 744−747. (d) Sisco, S. W.; Moore, J. S. Homochiral Self-Sorting of BINOL Macrocycles. *Chem. Sci.* **2014**, *5*, 81−85.

https://doi.org/10.1021/jacsau.2c00225
JACS Au 2022, 2, 1661−1668